13th International Symposium on Particle Image Velocimetry – ISPIV 2019
Munich, Germany, July 22-24, 2019

4D Digital Holographic PIV/PTV with 3D Volume Deconvolution and Predictive Inverse Reconstruction

Julio Soria[1*], Bihai Sun[1], Asif Ahmed[1] and Callum Atkinson[1]

[1] Laboratory for Turbulence Research in Aerospace & Combustion (LTRAC)
Department of Mechanical and Aerospace Engineering
Monash University (Clayton Campus)
Melbourne, VIC 3800 AUSTRALIA

[*] julio.soria@monash.edu

Abstract

Digital imaging array technology and processing power are continuously developing and have reached a state where 4-dimensional (*i.e.* time-resolved 3C-3D) digital holographic PIV/PTV (4D-DHPIV/PTV) methods can be considered for macro fluid mechanics and turbulence investigations. This paper presents an in-line 4D-DHPIV/PTV methodology, which in addition to including the standard digital hologram reconstruction, incorporates advanced digital filtering to remove the virtual image effect, 3-dimensional volume deconvolution to reduce the depth-of-focus problem and the virtual image, an efficient one-pass 3-dimensional clustering algorithm coupled with a new predictive inverse reconstruction approach based on previous work in this area, to increase the particle reconstruction dynamic range and 3-dimensional reconstruction domain. In addition to the presentation of the details of this 4D-DHPIV/PTV method, additional performance results pertaining to bias particle position error and uncertainty of the particle position are presented as a function of particle concentration.

1 Introduction

Most flows of relevance, both industrial and environmental, are three-dimensional (3D) in nature, highly unsteady, most likely high Reynolds number and therefore, turbulent in nature containing a large range of length scales and a large dynamic range. These characteristics necessitates a measurement technique to quantify and investigate these flows that is able to measure the instantaneous three-component three-dimensional (3C-3D) velocity vector with high spatial resolution in a time-accurate manner. Today this is still an exceedingly difficult task.

In the early days film-based holographic PIV (HPIV) was one of the methods that showed promise Barnhart et al. (1994); Hussain et al. (1993); Lozano et al. (1999); Ellenrieder et al. (2001), but due to its complex implementation it did not develop into a standard laboratory tool. More recently, digital holographic recording and reconstruction Coëtmellec et al. (2001); Murata and Yasuda (2000); Pan and Meng (2003); von Ellenrieder and Soria (2003); Lobera et al. (2004); Palero et al. (2007) coupled with cross-correlation PIV analysis (DHPIV) has shown promise as a 3C-3D velocity field measurement tool, but it too has its shortcoming, mainly due to the available size of sensor cells on current CCD/CMOS sensor arrays, which only permit in-line digital holographic recording. However, this limitations is becoming less severe as new CCD/CMOS sensor arrays are becoming available with micron and sub-micron sensor cells.

3D photogrammetry coupled with particle tracking has also only had limited success as a standard tool in the laboratory Malik et al. (1993b a); Sato et al. (1994) — primarily due to its complex calibration requirements. However, in the last decade photogrammetry has been coupled with cross-correlation PIV analysis in a technique now referred to as Tomographic PIV (TPIV) Ciofalo et al. (2003); Elsinga et al. (2006); Atkinson and Soria (2009). This technique uses multiple cameras, typically four digital cameras and requires a calibration similar to the stereo-PIV technique. TPIV can provide 3C-3D velocity fields of unsteady and/or turbulent flows although in its standard operational form, it suffers from severe limitations in spatial resolution Atkinson et al. (2011).

Apart from recording the three-dimensional position of tracer particles through the multiple view geometry of TPIV, there are other techniques that record the light-field information instead. One such technique

is synthetic aperture PIV (SAPIV), which uses a large camera array, typically 8–15 cameras, to capture the light-field images of seeding particles and reconstructs 3D particle images through a synthetic aperture refocusing method Belden et al. (2010). SAPIV can tolerate much higher particle densities than TPIV and its dynamic velocity measurement range along the optical axis can be of the same order as the lateral directions.

A recently developed alternative, instead of using a cumbersome camera array system, uses light-field imaging to record the particle light-field image via a single plenoptic camera Adelson and Wang (1992) which consists of a closely encapsulated micro-lens array (MLA) and a CCD/CMOS sensor. When coupled with cross-correlation PIV analysis we have a 3C-3D velocimetry technique, referred to as light-field PIV (LFPIV) Fahringer et al. (2015); Shi et al. (2017, 2018). LFPIV eliminates the cumbersome camera spatial calibration process, which is essential and a major source of error in TPIV. With a compact hardware setup similar as 2D-PIV, LFPIV is capable of measuring full volumetric 3C-3D velocity fields using a greatly simplified experimental procedure.

The three experimental methods which are commonly employed in Experimental Fluid Mechanics can be distinguish by their illumination source and inherent imaging method, classifying them either as *Incoherent Imaging* or *Coherent Imaging* methods. All photogrammetry methods such as TPIV and LFPIV belong to the Incoherent Imaging family because from a fundamental point of view they do not require a coherent light source such as a laser, with other illumination such as diode illumination Buchmann et al. (2012) sufficing to illuminate the fluid volume of interest that contains the scattering tracer particles. HPIV and more specifically DHPIV belong to the Coherent Imaging family and requires coherent illumination of a highly coherent laser to illuminate the fluid volume of interest containing the scattering tracer particles.

Common to all these methods is the fundamental source of the *3C velocity signal* at a point in 3D space. This signal is provided by the tracer particle or in fact many of them which are used to seed the fluid and which must provide a high-fidelity signal of the instantaneous 3C of the velocity vector at the location where the particle is located van Overbrüggen et al. (2016); Bosbach et al. (2008). This very important aspect in fluid flow velocimetry is not within the scope of this paper. The primary focus will be on the presentation of a 4-dimensional (*i.e.* time-resolved 3C-3D) digital holographic PIV/PTV (4D-DHPIV/PTV) methods that can be considered for macro fluid mechanics and turbulence investigations.

2 Digital Holographic PIV - Direct Reconstruction

DHPIV, using coherent imaging via digital holographic recording and digital holographic reconstruction, provides the 3D intensity field of all particles in a 3D volume directly from a single sensor and without the complex optical calibration which is essential in 3D fluid flow measurement methods like TPIV. Two sequentially recorded 3D intensity fields of all particles can subsequently be analysed using 3D cross-correlation analysis as is done in TPIV or a hybrid cross-correlation PIV - PTV approach can also be used Soria et al. (2014) to enhance the spatial resolution to the particle size level. The basic set-up for in-line digital hologram recording shown in figure 1 is described in Pan and Meng (2003); von Ellenrieder and Soria (2003); Palero et al. (2007). Note that the purpose of the lenses in the arranagment shown in figure 1 is to produce a collimated laser beam of sufficient diameter to illuminate the sample volume of interest and as a minimum the entire CCD/CMOS sensor.

This laser beam is used to illuminate sample objects, *e.g.* micron or sub-micron particles, as shown in figure 1. The laser light scatters from these particles, while the unobstructed laser light propagates to the CCD/CMOS sensor and acts as the reference laser illumination. The scattered laser light and that of the collimated reference beam interfere on the CCD sensor to form an interference pattern, which is referred to as the digital hologram.

The process of digital hologram reconstruction is, in principle, similar to the process of reconstructing an optical hologram. The hologram intensity distribution recorded on the electronic sensor, which is identified by the Cartesian coordinate system (x, y, z = 0), is multiplied by the reference (or its conjugate) wave and the resulting wave $I_H(x,y,0)$ is numerically propagated to the virtual (or real) image plane. The complex amplitude distribution $U(x_0,y_0;z)$ in any plane, which is a distance z normal from the hologram position, *i.e.* from the electronic sensor plane, can be calculated from $I_H(x,y,0)$ using the Rayleigh–Sommerfeld diffraction formula Goodman (1996),

$$U(x_0,y_0;z) = \frac{1}{\imath\lambda}\int_{\Sigma} I_H(x,y,0)\,\frac{\exp(\imath k r_{01})}{r_{01}}\cos(\vec{n},\vec{r_{01}})\,dxdy \tag{1}$$

where λ and $k=\frac{2\pi}{\lambda}$ is the wavelength and wavenumber respectively of the illumination used during the recording of the digital hologram. $r_{01}=\sqrt{(x-x_0)^2+(y-y_0)^2+z^2}$ is the distance from a point $(x,y,0)$

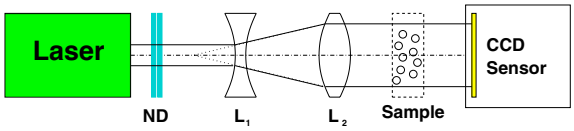

Figure 1: Typical experimental arrangement for in-line digital hologram recording (plan view), ND = neutral density filter, L_1 = diverging spherical lens, L_2 = converging lens.

on the electronic sensor to any point (x_0, y_0, z) in the reconstructed image plane identified by the distance z from the electronic sensor with $\vec{n}$ the outward unit normal of the diffraction surface Goodman (1996). The obliquity factor $\cos(\vec{n}, \vec{r_{01}})$ for most practical applications can be readily approximated by

$$\cos(\vec{n}, \vec{r_{01}}) \approx 1 \tag{2}$$

for typical dimensions involved in digital hologram recording. This permits equation (1) to be written as the convolution integral

$$U(x_0, y_0; z) = \int_{\Sigma} I_H(x, y, 0)\, h(x_0, y_0, z; x, y)\, dx\, dy \tag{3}$$

which is interpreted as the convolution between $I_H(x, y, 0)$ and the diffraction kernel given by:

$$h(x_0, y_0, z; x, y) = \frac{\exp(\imath k r_{01})}{\imath \lambda r_{01}} \tag{4}$$

Defining the Fourier transforms, $\mathcal{F}[\,]$, of $I_H(x, y, 0)$ and the diffraction kernel by

$$\begin{aligned} I_H(f_x, f_y) &= \mathcal{F}[I_H(x, y, 0)] \\ H(f_x, f_y; z) &= \mathcal{F}[h(x_0, y_0, z; x, y)] \end{aligned} \tag{5}$$

respectively, allows the complex amplitude distribution in the image plane to be numerically calculated in an efficient way using

$$U(x_0, y_0; z) = \mathcal{F}^{-1}[I_H(f_x, f_y) H(f_x, f_y; z)] \tag{6}$$

where $\mathcal{F}^{-1}$ represents the inverse Fourier transform. In practice the Fast Fourier transform is used to compute equations (5) and (6).

In the digital hologram reconstruction approach using equation (6) the method developed by Onural and Scott (1987) is recursively implemented to determine the reconstructed planar image intensities of the particles in several closely spaced planes normal to the z-coordinate direction, where the spacing of these planes should correspond to the in-plane spatial resolution. The Onural and Scott (1987) technique utilizes an iterative filter that limits the twin-image effect (*i.e.* the real and virtual images), common to all in-line holograms, by averaging.

Figure 2 illustrates the results of the different stages: (a) is an example of a digitally recorded hologram while (b) shows the intensity cross-sections of a particle (indicated in (a)) as a function of reconstruction distance z_0 from the sensor. Figure 2 (c) shows the diameter variation as a function of z_0, clearly indicating that the reconstructed diameter varies by less than 3% from a value of 140 μm over a domain of z_0 equal to 2.4 mm, which is clearly not physical. Figure 2 (c) also shows the standard deviation of the reconstructed image intensity, σ_i plotted as a function of the distance z_0 from the CCD sensor (Δz_0= 0.1 mm). The minimum of σ_i occurs at –88.8 mm and the droplet size at this position is 140.1 μm, which identifies the particle diameter.

The particle elongation demonstrated in Figure 2 had been previously observed by von Ellenrieder and Soria (2003) among others, who found that the digital reconstruction of digital in-line holograms described above reconstructs particles of 90 μm diameter with an estimated linear out-of-plane dimension of approximately 15.2 mm, (*i.e.* the ellipsoidal major axis of the reconstructed particle is in the z-coordinate direction) as shown in figure 3. This effect is known as the depth-of-field problem of in-line holography von Ellenrieder and Soria (2003). Possible means of overcoming the depth-of-field problem suggested by von Ellenrieder and Soria (2003) include particle side scattering, off-axis holography and the tomographic approach to DH-PIV proposed by Soria and Atkinson (2008).

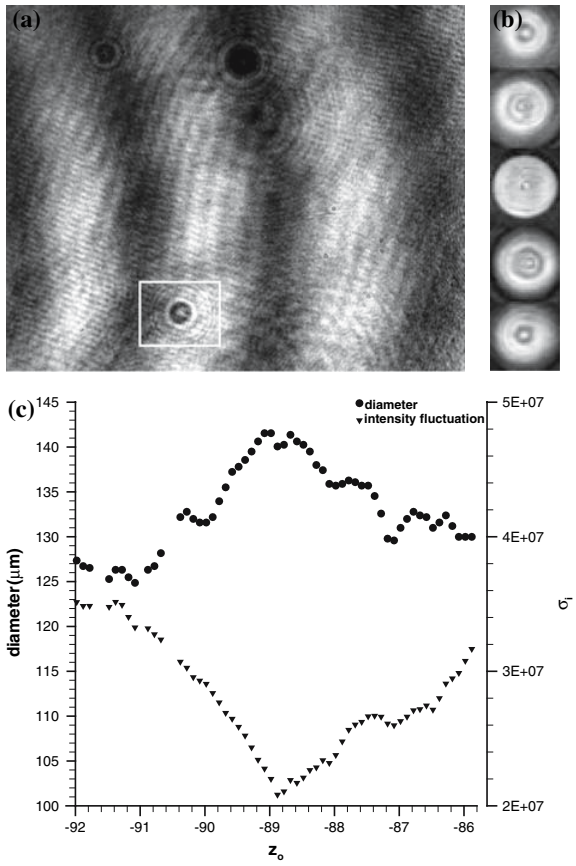

Figure 2: (a) Digital in-line hologram, (b) reconstructed particle for z_0 ranging from –85 to –93 mm, (c) particle diameter and standard deviation of the reconstructed image intensity as a function of z_o.

The use of side scatter requires optical elements that add complexity and can possibly distort the particle images. Furthermore, this approach requires more powerful lasers than required for in-line holography, typically going from milli-Watts to 100 Watts. Off-axis holography, on the other hand, also has its limitations: the angle-dependent wavenumber of the interference pattern formed by the reference and object beams during off-axis hologram recording is $\zeta = \frac{\sin\theta}{\lambda}$. The maximum wavenumber that can be resolved by the CCD/CMOS array sensor is the inverse of twice the pixel size: $\zeta_{max} \approx \frac{1}{2\Delta}$. For typical CCD/CMOS array sensor, which have a pixel size of 6-7 μm and Nd:YAG laser illumination with a wavelength $\lambda = 532nm$, this yields a maximum angle of about $\theta_{max} \approx 2.1^0$. However, in order to separate the real and virtual images a minimum angle of $\theta_{min} = \sin^{-1}(B\lambda)$ is required (where B is the maximum spatial frequency of the image). For PIV applications, given sparse seeding and large particles these competing effects can be satisfied, but only for a small object field that is located relatively far away from the CCD/CMOS array sensor. This severely limits the application of off-axis holographic recording in macro Fluid Mechanics experiments and for these flows in-line DHPIV is the hologram recording method of choice. A number of recent additional approaches that overcome the depth-of-field problem of in-line holography use a magnification Nguyen et al. (2011) or microscopy Sheng et al. (2008) approach to record a magnified hologram. However, this approach comes at the expense of the proportionally reduced spatial domain that can be measured.

From a fundamental point of view DHPIV is an appealing 3C-3D PIV/PTV techniques with the main advantage that this approach does not require any optical calibration and inherently does introduce optical distortions. It simply requires a low-energy coherent laser, two lenses to enlarge the laser beam into a collimated beam that encompasses the flow domain of interest and a relatively large digital sensor with small pixels. With respect to the latter, large sensor arrays of the order of 50 MPx are becoming available with a

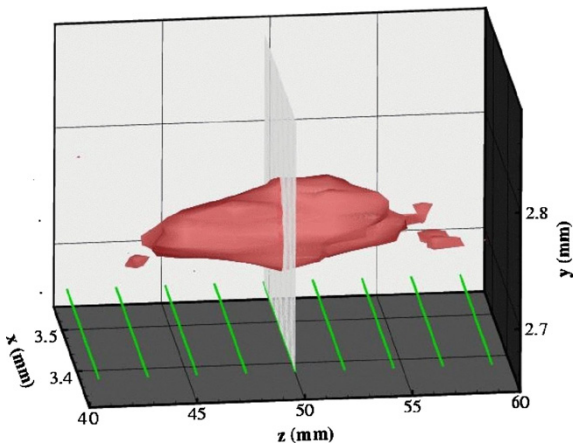

Figure 3: Digital hologram reconstruction of a 90 μm diameter particle recorded using in-line digital holography. The central plane at z = 49.7 mm is shown as a grey sheet and the green lines correspond to the locations of the other reconstruction planes von Ellenrieder and Soria (2003).

pixels size of 5.5 μm. When coupled with a 10X microscope in a micro-DHPIV arrangement Nguyen et al. (2011), the effective pixel size is of the order of the typical laser illuminating wavelength, *e.g.* $\lambda = 532\ nm$, enabling the instantaneous 3C-3D fluid velocity vector field measurement in a fluid volume with a typical projected area of 5 mm x 3 mm at the spatial resolution of the wavelength of the laser. Therefore, even from the point of view of spatial resolution, DHPIV is unsurpassed by its direct competitors like TPIV or LFPIV.

3 Digital Holographic PIV - Advanced Reconstruction Approach

A number of the shortcomings of the direct digital hologram reconstruction can be overcome by implementing additional processes in an iterative approach. The first additional process is to apply a three-dimensional (3D) deconvolution step introduced by Latychevskaia et al. (2010) using a point-spread function (PSF) to the direct hologram reconstruction, which reconstruct the true 3D amplitude distribution of objects. This 3D-deconvolution restores the positions of volume-spread objects such as the small particles used in PIV. The PSF required for 3D-deconvolution can either be obtained by experimentally recording and reconstructing a hologram of an arbitrarily small individual scatterer or as the reconstruction of a simulated hologram of a point scatterer. The application of 3D-deconvolution brings the out-of-focus signal back to its scatterer and automatically removes the twin image as it is not part of the scattered wave. This results in spatially well localised particles free from artefacts. Mathematically, this process is given by (7):

$$U_{Real}(x_0, y_0; z) = \mathcal{F}^{-1}\left[\frac{\mathcal{F}\left[U(x_0, y_0; z)\right]}{\mathcal{F}\left[U_{PSF}(x, y, z)\right]}\right] \tag{7}$$

where $U_{Real}(x_0, y_0; z)$ is the 3D-deconvolved complex amplitude distribution and $U_{PSF}(x, y, z)$ is the 3D point-spread function.

Figure 4 (a) shows the result of a direct reconstruction and the effect of the virtual out-of-focus particle on the real particle reconstruction. Figure 4 (b) shows the appropriate computed PSF, while (c) shows the 3D-deconvolved reconstructed particle intensity field, showing the vastly improved localisation of the particle intensities.

The contribution of the 3D intensity field to individual reconstructed particles is obtained via an efficient one-pass 3-dimensional Hoshen Kopelman (HK) clustering algorithm Hoshen and Kopelman (1976). The result from this clustering algorithm is then coupled with a novel iterative predictive inverse reconstruction approach Soulez et al. (2007) to further improve the location of the particles, as well as detect particles which are either in the shadow of particles, are weak scatters or are in fact outside the projected area of the sensor. The iterative hologram reconstruction approach includes: (i) direct digital hologram reconstruction followed by (ii) 3D-deconvolution, (iii) HK particle clustering, (iv) inverse reconstruction, (v) digital hologram generation, (vi) subtraction of the digital hologram of the reconstructed particles to reveal the

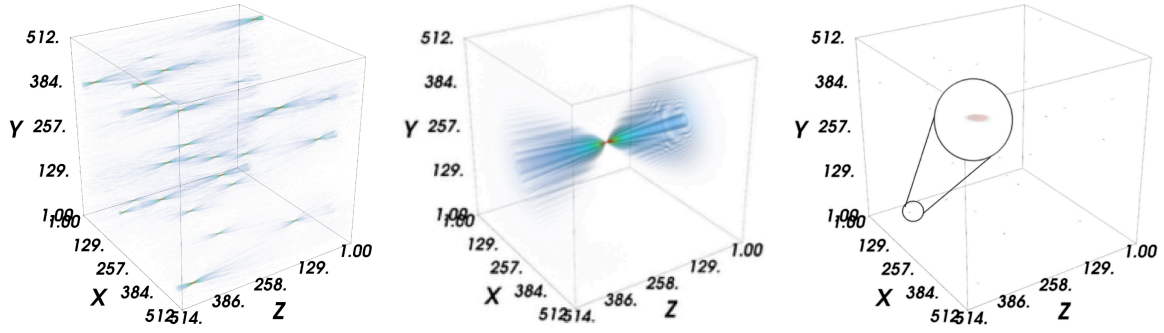

(a) (b) (c)

Figure 4: (a) Typical 3D direct hologram reconstruction of particles, (b) point-spread function, (c) 3D-deconvolved reconstruction of particles.

holograms of further particles, etc. These processes are illustrated in fig. 5. The iterative process is iterated until a residual hologram is at the noise level.

Once a sequential pair of 3D holograms has been reconstructed, these can be analysed using 3D cross-correlation analysis or a hybrid cross-correlation PIV - PTV at the particle spatial resolution level Soria et al. (2014) to reveal the 3C-3D fluid velocity field. Furthermore, since a time series of digital holograms is available in this 4D-DHPIV/PTV methodology, then once 3-4 3C-3D velocity fields are available, quite accurate predictive positions of the particle locations can be used to accelerate the inverse hologram reconstruction step in fig. 5. An example of the result of the iterative hologram reconstruction approach described via fig. 5 is shown in fig. 6 based on a digitally generated hologram using particles that are randomly distributed within a volume.

4 Analysis of the Effect of Particle Concentration on Iterative Hologram Reconstruction

The effect of particle concentration on the iterative hologram reconstruction as measured by the bias error and uncertainty of the particle centroid location has been investigated. For this numerical study the wavelength of the coherent laser illumination was set at $\lambda = 532\,nm$. Particles where randomly distributed in a volume of $64\,\mu m \times 64\,\mu m \times 109\,\mu m$ where the largest dimension is the out-of-plane z-direction normal to the recording sensor surface. The particles had a diameter uniformly distributed between $1.5 - 2.5\,\mu m$ ($\sim 2.82\lambda - 4.7\lambda$). The number of particles used within this volume was 10, 20, 30, 40, 50 and 80, resulting in corresponding particle concentrations of 2.2×10^{-5}, 4.5×10^{-5}, 6.7×10^{-5}, 9.0×10^{-5}, 1.1×10^{-4}, 1.8×10^{-4} particles/μm^3. Except for the 80 particles per volume case 18,000 numerical samples were produced and analysed. For the 80 particle per volume case 7,814 numerical samples were produced and analysed.

Figure 7 shows the percentage of correct particles detected using direct hologram reconstruction and iterative hologram reconstruction as a function of particle concentration. These results show the superior performance of the iterative hologram reconstruction approach, which significantly outperforms the direct hologram reconstruction method by correctly identifying more than 70% of all particles even for high particle concentration, whereas the direct method at the lowest concentration detects at best 35% of all particles. Only for the highest particle concentration does the detection drop to 40% of all particles for the iterative hologram reconstruction approach. However, for this concentration the direct hologram reconstruction is only able to detect one order less at around 4% of all particles. It is noteworthy to realise that a concentration of 1.1×10^{-4} particles/μm^3 corresponds to 110,000 particles in 1 mm^3, whereas the highest concentration used here of 1.8×10^{-4} particles/μm^3 corresponds to 180,000 particles in 1 mm^3, which is an exceedingly high particle concentration.

Figure 8 shows (a) the normalized bias error and (b) normalised standard uncertainty of the particle centroid position in the in-plane (x,y) directions and the out-of-plane z direction using iterative hologram reconstruction. The normalisation is with respect to the illumination wavelength $\lambda = 532\,nm$. The bias error of the centroid position is typically less that 0.25λ for the in-plane coordinates for all particle concentrations

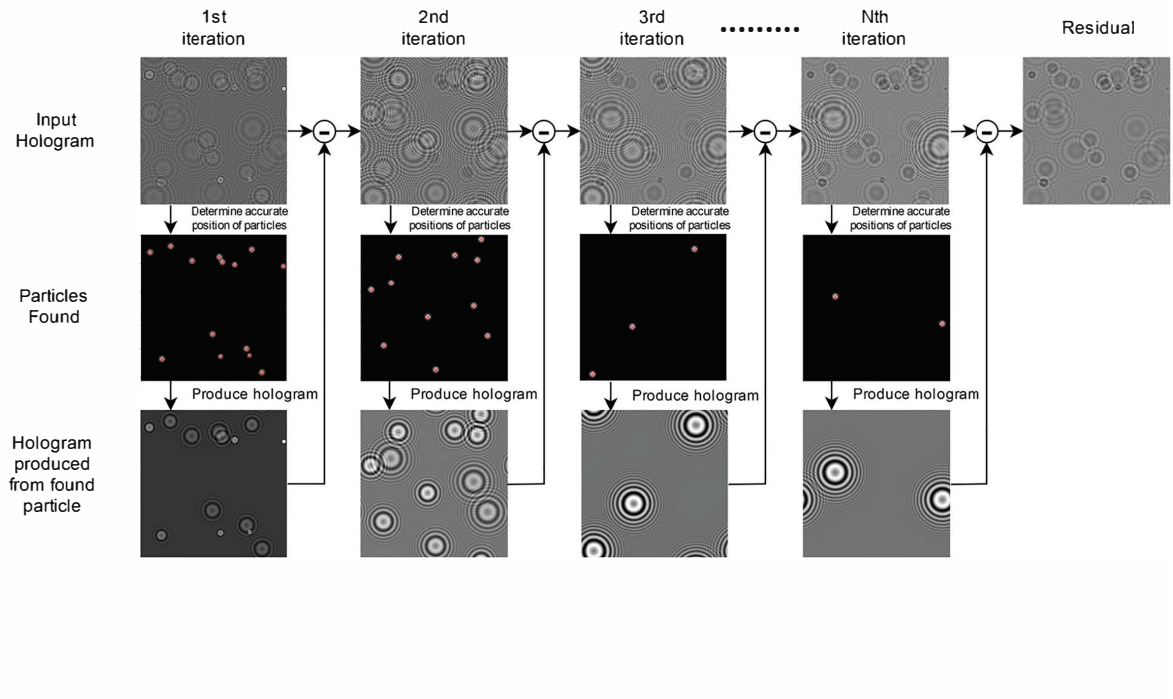

Figure 5: Iterative 3D Hologram reconstruction approach.

used in this study, characterised by an underestimation. The bias error in the out-of-plane position is of the same order as the in-plane except for the lowest and highest concentration, where the bias error is found to be at most 1.5λ, characterised by underestimation and overestimation.

The standard uncertainty shown in fig. 8 (b) does not exceed 3.5λ for the in-plane particle centroid coordinates with a minimum at the concentration of 4.5×10^{-5} particles/μm^3 of less than 2λ. The standard uncertainty for the out-of-plane particle centroid coordinate is significantly higher of the order of 8λ or less except for the highest concentration where the standard uncertainty peaks at slightly above 12λ. The variation of the standard uncertainty for the out-of-plane particle centroid coordinate shadows the in-plane standard uncertainties but with more of a minimum plateau between the particle concentrations of $4.5 \times 10^{-5} - 9.0 \times 10^{-5}$ particles/μm^3.

5 Concluding Remarks

This paper describes the details of direct digital hologram reconstruction and discusses some of its shortcomings. An in-line 4-dimensional (*i.e.* time-resolved 3C-3D) digital holographic PIV/PTV (4D-DHPIV/PTV) method is presented which overcomes these shortcomings. This 4D-DHPIV/PTV method, in addition to including the standard digital hologram reconstruction, incorporates advanced digital filtering to remove the virtual image effect, 3-dimensional volume deconvolution to reduce the depth-of-focus problem and the virtual image, an efficient one-pass 3-dimensional HK clustering algorithm coupled with a novel predictive inverse reconstruction approach based on previous work in this area.

A numerical study has been undertaken to investigate bias particle position error and standard uncertainty of the particle position as a function of particle concentration. The particle concentrations used in this study ranged from $2.2 \times 10^{-5} - 1.8 \times 10^{-4}$ particles/μm^3, the highest particle concentration corresponding

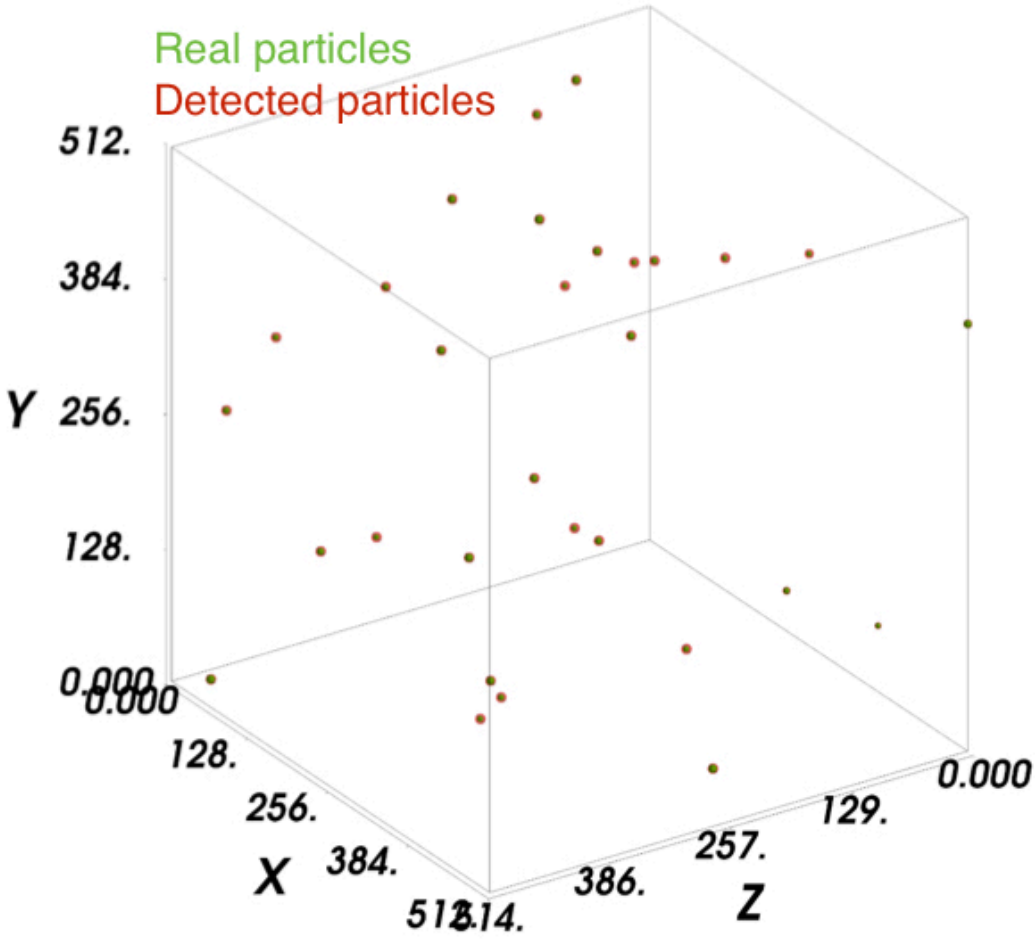

Figure 6: Example illustrating the result of iterative 3D Hologram reconstruction.

to 180,000 particles in 1 mm^3. This study has found that the iterative hologram reconstruction of the 4D-DHPIV/PTV can detect 70% of all particles even for high particle concentration, whereas the direct method at the lowest concentration detects at best 35% of all particles. Only for the highest particle concentration of 1.8×10^{-4} particles/μm^3 does the detection drop to 40% of all particles for the iterative hologram reconstruction approach. The bias error of the centroid position is typically less that 0.25λ for the in-plane coordinates for all particle concentrations used in this study, while for the out-of-plane position, it is of the same order as the in-plane except for the lowest and highest concentration, where the bias error is found to be at most 1.5λ. The standard uncertainty does not exceed 3.5λ for the in-plane particle centroid coordinates with a minimum of less than 2λ at the concentration of 4.5×10^{-5} particles/μm^3. However, The standard uncertainty for the out-of-plane particle centroid coordinate is significantly higher of the order of 8λ or less except for the highest concentration where the standard uncertainty peaks at slightly above 12λ.

Acknowledgements

The authors would like to acknowledge the research funding from the Australian Government through the Australian Research Council. J. Soria gratefully acknowledges the support of an Australian Research Council Discovery Outstanding Researcher Award fellowship. C. Atkinson was supported by the ARC Discovery Early Career Researcher Award (DECRA) fellowship. This work was also supported by the computational resources provided by The Pawsey Supercomputing Centre and the National Computational Infrastructure

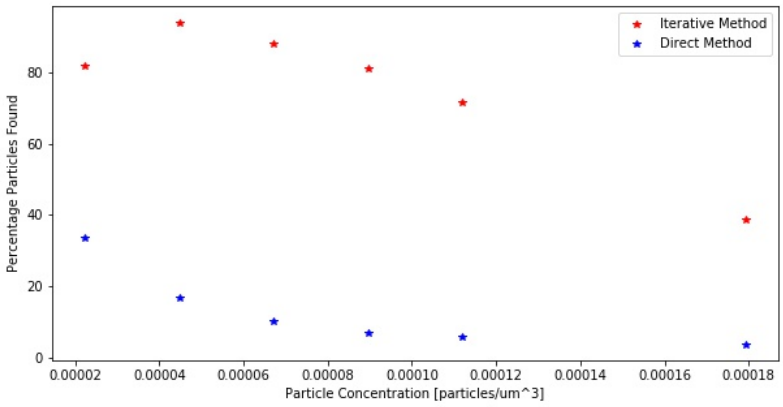

Figure 7: Percentage correct particles found using direct hologram reconstruction and iterative hologram reconstruction as a function of particle concentration.

through the National Computational Merit Allocation Scheme (NCMAS) funded by the Australian Government.

References

Adelson EH and Wang JYA (1992) Single Lens Stereo with a Plenoptic Camera. *IEEE Transactions on Pattern Analysis and Machine Intelligence* 14:99–106

Atkinson C, Coudert S, Foucaut JM, Stanislas M, and Soria J (2011) The accuracy of tomographic particle image velocimetry for measurements of a turbulent boundary layer. *Experiments in fluids* 50:1031–1056

Atkinson C and Soria J (2009) An efficient simultaneous reconstruction technique for tomographic particle image velocimetry. *Experiments in Fluids* 47:553–568

Barnhart D, Adrian R, and Papen G (1994) Phase-conjugate holographic system for high resolution particle image velocimetry. *Applied Optics* 33:7159–7170

Belden J, Truscott TT, Axiak MC, and Techet AH (2010) Three-dimensional synthetic aperture particle image velocimetry. *Measurement Science and Technology* 21:5403

Bosbach J, Kühn M, and Wagner C (2008) Large scale particle image velocimetry with helium filled soap bubbles. *Experiments in Fluids* 46:539–547

Buchmann NA, Willert CE, and Soria J (2012) Pulsed, high-power LED illumination for tomographic particle image velocimetry. *Experiments in Fluids* 53:1545–1560

Ciofalo M, Signorin M, and Simiano M (2003) Tomographic particle-image velocimetry and thermography in Rayleigh-Banard convection using suspended thermochromic liquid crystals and digital image processing. *Experiments in Fluids* 34:156–172

Coëtmellec S, Buraga-Lefebvre C, Lebrun D, and Özkul C (2001) Application of in-line digital holography to multiple plane velocimetry. *Measurement Science and Technology* 12:1392–1397

Ellenrieder Kv, Kostas J, and Soria J (2001) Measurements of a wall-bounded turbulent, separated flow using HPIV. *Journal of Turbulence* 2:1–15

Elsinga GE, Scarano F, Wieneke B, and Van Oudheusden B (2006) Tomographic particle image velocimetry. *Experiments in Fluids* 41:933–947

Fahringer TW, Lynch KP, and Thurow BS (2015) Volumetric particle image velocimetry with a single plenoptic camera. *Measurement Science and Technology* 26:115201

Goodman JW (1996) *Introduction to Fourier Optics*. McGraw-Hill. second edition edition

Hoshen J and Kopelman R (1976) Percolation and cluster distribution. I. Cluster multiple labeling technique and critical concentration algorithm. *Physical Review B (Solid State)* 14:3438–3445

Hussain F, Liu DD, Simmonds S, and Meng H (1993) Hpiv prospects and limitations holographic particle image velocimetry. *FED* 148:1–11

Latychevskaia T, Gehri F, and Fink HW (2010) Depth-resolved holographic reconstructions by three-dimensional deconvolution. *Optics Express* 18:22527

Lobera J, Andrés N, and Arroyo MP (2004) Digital speckle pattern interferometry as a holographic velocimetry technique. *Measurement Science and Technology* 15:718–724

Lozano A, Kostas J, and Soria J (1999) Use of holography in particle image velocimetry measurements of a swirling flow. *Experiments in Fluids* 27:251—261

Malik N, Dracos T, and Papantoniou D (1993a) PTV in 3-D flows; Part II : Particle Tracking. *Experiments in Fluids* 15:279–294

Malik NA, Dracos T, and Papantoniou DA (1993b) Particle tracking velocimetry in three-dimensional flows. *Experiments in Fluids* 15:279–294

Murata S and Yasuda N (2000) Potential of digital holography in particle measurement. *Optics and Laser Technology* 32:567–574

Nguyen D, Honnery D, and Soria J (2011) Measuring evaporation of micro-fuel droplets using magnified DIH and DPIV. *Experiments in Fluids* 50:949–959

Onural L and Scott PD (1987) Digital decoding of in-line holograms. *Optical Engineering* 26:1124–1132

Palero V, Arroyo MP, and Soria J (2007) Digital holography for micro-droplet diagnostics. *Experiments in Fluids* 43:185–195

Pan G and Meng H (2003) Digital holography of particle fields: reconstruction by use of complex amplitude. *Applied Optics* 42:827–833

Sato YK, Kasagi N, and Takamura N (1994) Application of the three-dimensional particle tracking velocimeter to a turbulent air ßow. in *Proceedings of third Asian Symposium on Visualization*. pages 705 – 709

Sheng J, Malkiel E, and Katz J (2008) Using digital holographic microscopy for simultaneous measurements of 3D near wall velocity and wall shear stress in a turbulent boundary layer. *Experiments in Fluids* 45:1023–1035

Shi S, Ding J, Atkinson C, Soria J, and New TH (2018) A detailed comparison of single-camera light-field PIV and tomographic PIV. *Experiments in Fluids* 59:1690

Shi S, Ding J, New TH, and Soria J (2017) Light-field camera-based 3D volumetric particle image velocimetry with dense ray tracing reconstruction technique. *Experiments in Fluids* 58:78

Soria J and Atkinson C (2008) Towards 3C-3D digital holographic fluid velocity vector field measurement—tomographic digital holographic PIV (Tomo-HPIV). *Measurement Science and Technology* 19:4002

Soria J, Atkinson C, and Buchmann N (2014) Hybrid PIV-Particle Tracking technique applied to high Reynolds number turbulent boundary layer measurements. in *67th Annual Meeting of the APS Division of Fluid Dynamics Meeting of The American Physical Society*

Soulez F, Denis L, Thiébaut É, Fournier C, and Goepfert C (2007) Inverse problem approach in particle digital holography: out-of-field particle detection made possible. *Journal of the Optical Society of America A* 24:3708–1171

van Overbrüggen T, Klaas M, Soria J, and Schröder W (2016) Experimental analysis of particle sizes for PIV measurements. *Measurement Science and Technology* 27:094009

von Ellenrieder K and Soria J (2003) Experimental measurements of particle depth of field in digital holography. in *International Workshop on Holographic metrology in Fluid Mechanics*

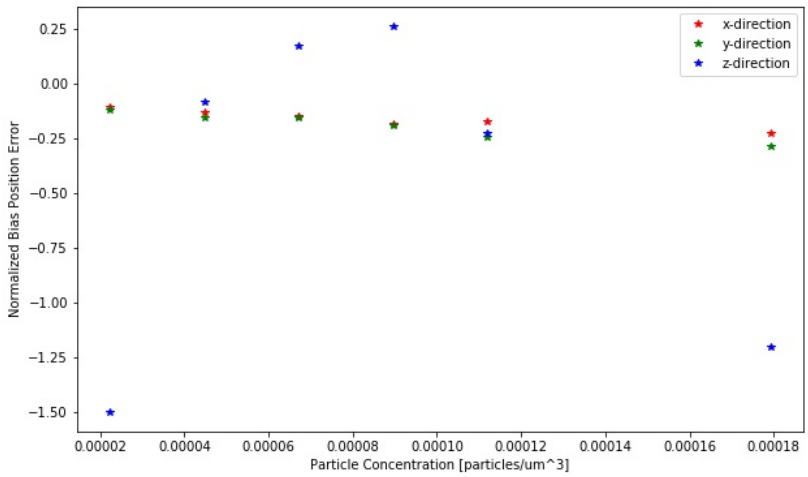

(a)

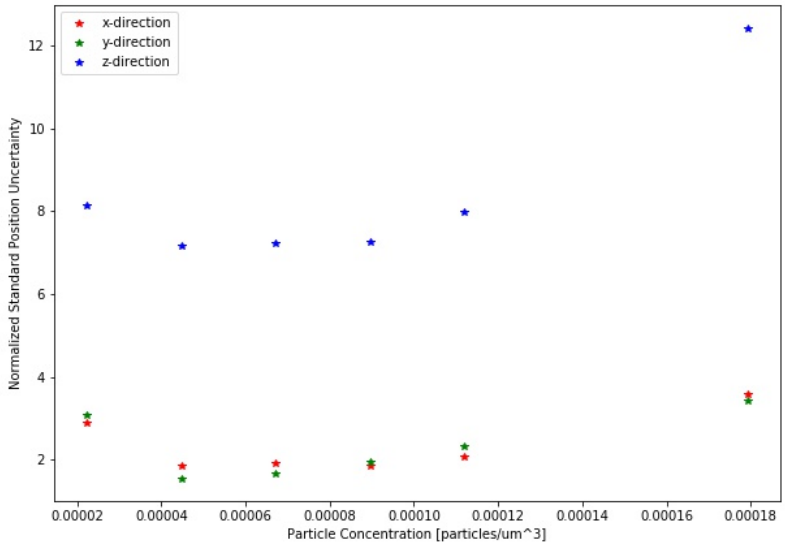

(b)

Figure 8: Precision and uncertainty in the particle centroid position using iterative hologram reconstruction. (a) Normalised bias error, (b) normalised standard uncertainty. Normalisation is with respect to the wavelength $\lambda = 532\,nm$.